International Journal of Heat and Technology
Vol. 44, No. 3, June, 2026, pp. 945-957
Journal homepage: http://iieta.org/journals/ijht

Multiscale Analysis of Irreversible Thermodynamic Processes and Entropy Production Laws at Light-Metal Surface-Treatment Interfaces

Changsheng Liu[1*], Kanghong Chen[2], Wenbi Zhang[2], Zhiguan Yi[2]

[1] School of Xinchang, Zhejiang Industry Polytechnic College, Shaoxing 312000, China
[2] Hangzhou Win-Win Technology CO., LTD, Hangzhou 311500, China

Corresponding Author Email: stevenl20088@126.com

https://doi.org/10.18280/ijht.440304

Received: 12 January 2026
Revised: 7 May 2026
Accepted: 22 May 2026
Available online: 30 June 2026

Keywords:
light metals, surface treatment, irreversible thermodynamics, entropy production laws, multiscale analysis, interfacial anisotropy, process optimization

ABSTRACT

During the surface treatment of light metals, the irreversible interfacial behavior and energy dissipation characteristics directly determine coating quality and process energy efficiency. Existing thermodynamic studies, due to their limitations, cannot accurately reveal the intrinsic mechanisms underlying multiscale irreversible interfacial evolution. In this work, a multiscale irreversible-thermodynamic framework tailored to light-metal interfacial modification was established. Based on Gibbs excess theory, the physical mechanisms of interfacial entropy production were decoupled and decomposed across spatial scales, enabling quantitative differentiation of irreversible dissipation contributions from in-plane evolution and cross-interface transport and achieving refined characterization of entropy-production features at atomic, mesoscopic, and macroscopic levels. With global positive definiteness of entropy production as the core constraint, a thermodynamically self-consistent cross-scale information-transfer mechanism was established via variational principles, and the constitutive relations between generalized forces and fluxes at each scale were derived. Incorporating the anisotropic characteristics of hexagonal close-packed crystal structures, an orientation-degree-of-freedom was introduced into the mesoscopic entropy-production model to elucidate the regulatory effects of crystallographic orientation on interfacial energy dissipation and morphological evolution. Through a hierarchically coupled approach integrating first-principles calculations, phase-field modeling, and finite-element simulations, multiscale entropy-production maps were constructed for typical anodizing and micro-arc oxidation processes, systematically dissecting the distinct dissipative mechanisms. The theoretical model was rigorously validated via multiple controlled experiments, and thermodynamic optimization criteria for light-metal surface-treatment processes were established based on the principle of minimum entropy production. The results indicate that the total interfacial entropy production is governed jointly by localized in-plane irreversible processes and cross-interface multifield transport; crystallographic anisotropy significantly alters the spatial distribution of mesoscopic entropy production; and multiscale coarse-graining strictly follows a monotonic decrease in entropy production. This study enriches the nonequilibrium thermodynamic theory for anisotropic light-metal interfaces and provides a theoretical foundation for the development of low-energy, high-quality surface-modification processes and the precise optimization of processing parameters.

1. INTRODUCTION

Lightweight metal alloys, owing to their superior specific strength, thermal conductivity, and formability, have been established as core structural materials in high-end manufacturing sectors, including aerospace equipment, rail transit components, precision electronic packaging, and biomedical devices [1, 2]. Constrained by their inherently high chemical reactivity, light metal substrates generally suffer from intrinsic deficiencies such as inadequate corrosion resistance and insufficient surface mechanical properties, which substantially limit their long-term service stability and broaden engineering applications [3, 4]. Various surface modification technologies, through the construction of functional protective coatings on the substrate surface, constitute the primary technical approach for enhancing the surface performance of light metals and extending the service life of components [5, 6]. Practical surface modification processes invariably operate under nonequilibrium thermodynamic states, wherein multiple physical fields—including heat transfer, mass transport, electrochemical reactions, and interfacial phase transformations—are strongly coupled, and both the overall energy dissipation and interfacial evolution belong to typical irreversible processes [7, 8]. Accurate elucidation of the irreversible evolution mechanisms inherent in such nonequilibrium systems, together with quantitative characterization of the distribution features and dynamic evolutionary patterns of interfacial entropy production, enables the interpretation of coating growth and defect formation mechanisms from a fundamental thermodynamic perspective, thereby providing solid theoretical support for improving process energy efficiency and regulating coating quality. Irreversible process thermodynamics serves as the core theoretical tool for analyzing the evolutionary behavior of nonequilibrium systems, by which the degree of irreversible dissipation can be quantitatively characterized through the entropy production rate, and has been extensively applied in research fields such as electrochemistry, heat and mass transfer, and material interfacial evolution [9, 10]. However, light metal surfaces and interfaces possess distinctive structural and physicochemical characteristics, including the independent thermodynamic properties of finite-thickness interfacial layers, the spanning of interfacial evolution across multiple spatial scales, and the crystallographic-orientation-induced thermodynamic anisotropy. These features render conventional thermodynamic theories inadequate for accurately depicting the irreversible evolutionary behavior, necessitating the establishment of a multiscale nonequilibrium thermodynamic analytical framework that is specifically adapted to the characteristics of light metal interfaces [11, 12].

Current thermodynamic investigations of light-metal surface-treatment processes, both domestically and internationally, still suffer from numerous critical deficiencies that hinder the deepening of process mechanisms and the realization of precise optimization. In existing thermodynamic analyses, idealized interfacial assumptions are generally adopted, wherein solid–liquid and solid–gas interfaces are simplified as zero-thickness geometric surfaces, with the microscopic structure and independent thermodynamic responses of the interfacial layer being completely neglected [13, 14]. Although certain studies have attempted to extend the equilibrium Gibbs excess theory to nonequilibrium systems, acknowledging the physical characteristics of the interface as an independent two-dimensional thermodynamic phase, a systematic and universal framework for characterizing the interfacial entropy production rate under the complex, multifield-coupled conditions typical of light-metal surface treatment has yet to be established. At the level of multiscale simulation research, mainstream computational approaches—including first-principles calculations, molecular dynamics, and finite-element methods—have focused exclusively on the fitting and matching of mechanical properties and transport parameters across different scales [15, 16], while entirely disregarding the core constraint imposed by the second law of thermodynamics on cross-scale information transfer. Consequently, the coarse-graining procedures at various scales fail to guarantee the non-negativity of the entropy production rate [17, 18], resulting in thermodynamic inconsistency within the multiscale models and substantially compromising the physical rigor and predictive accuracy of the theoretical frameworks. Moreover, existing studies generally overlook the anisotropic characteristics of light-metal crystal structures; for materials such as hexagonal close-packed magnesium alloys, core thermodynamic parameters, including surface energy and diffusion coefficients, exhibit pronounced orientation dependence [19, 20]. Although certain anisotropic thermodynamic theories have been developed, their application has been confined to the analysis of interfacial morphological evolution, without establishing quantitative correlations between crystallographic orientation and entropy production laws under actual surface-treatment engineering conditions. Simultaneously, a pronounced disconnection between theory and engineering practice persists in contemporary entropy-production research, wherein entropy production is employed merely as a qualitative indicator for elucidating energy dissipation mechanisms, without constructing standardized and implementable process optimization systems grounded in entropy-variation principles. This situation precludes the full exploitation of the engineering application value inherent in irreversible thermodynamic theory [21].

In response to the aforementioned research bottlenecks, a multiscale irreversible thermodynamic analytical framework centered on the entropy production rate is constructed, forming a four-in-one systematic innovation system. Based on the Gibbs excess theory, the physical mechanisms of interfacial entropy production are decomposed and quantitatively resolved across multiple scales, enabling precise decoupling of irreversible interfacial dissipation. Through the variational method, a cross-scale information-transfer mechanism satisfying the positive-definiteness constraint of entropy production is established, thereby resolving the thermodynamic inconsistency inherent in multiscale models. By introducing interfacial rotational degrees of freedom, an orientation-dependent mesoscopic entropy-production model is developed to accurately characterize the irreversible evolutionary behavior of anisotropic interfaces. Through the integration of numerical simulations and experimental measurements, entropy-production maps are constructed, and standardized process optimization criteria are established based on the principle of minimum entropy production, achieving a deep integration of nonequilibrium thermodynamic theory with engineering applications in light-metal surface treatment.

A progressively layered research architecture is adopted to systematically complete the entire workflow encompassing theoretical derivation, model construction, numerical simulation, and experimental validation. The foundational theories of irreversible thermodynamics and interfacial thermodynamics are successively laid out in individual chapters, followed by the progressive development of core research contents, including multiscale decomposition of interfacial entropy production, construction of a thermodynamically self-consistent cross-scale framework, and establishment of anisotropic entropy-production models. Engineering validation of the theoretical models is conducted through two representative process routes—anodizing and micro-arc oxidation—and the concluding section synthesizes the overall research findings while outlining directions for future investigation.

2. MULTISCALE DECOMPOSITION OF INTERFACIAL EXCESS ENTROPY PRODUCTION RATE BASED ON THE GIBBS EXCESS METHOD

The solid–liquid and solid–gas interfaces formed during light-metal surface modification processes possess finite physical thicknesses, and their internal microstructures and thermodynamic responses are fundamentally distinct from those of the material bulk phase. Consequently, the conventional zero-thickness geometric interface assumption fails to accurately capture the nonequilibrium evolutionary characteristics of the interfacial region. Based on the Gibbs excess thermodynamic theory, the interfacial region is defined as a two-dimensional functional phase with independent thermodynamic properties, thereby enabling the decoupling of thermodynamic behaviors between the bulk region and the interfacial region. A schematic illustration of the decoupling of multiple physical mechanisms and the multiscale decomposition of the interfacial excess entropy production rate for light-metal interfaces is presented in Figure 1. Within the total spatial domain of the system, the total entropy can be expressed as the linear superposition of the intrinsic bulk entropy and the interfacial excess entropy, with the corresponding quantitative relationship given by $S=S_b+S_s$. In conjunction with the entropy balance criterion of nonequilibrium thermodynamics, the overall entropy production rate of the system can be formulated through partitioned integration over the bulk and interfacial regions, as expressed by:

$$\dot{S}=\int_{V_b}\sigma_b\ dV+\int_{A_s}\sigma_s\ dA \quad (1)$$

where, V_b denotes the volume of the material bulk phase, A_s denotes the effective interfacial area, the scalar σ_b represents the volumetric entropy production rate of the bulk phase, which characterizes the irreversible dissipation arising from heat and mass transport within the bulk medium, and σ_s denotes the areal excess entropy production rate of the interface, specifically characterizing the energy dissipation behavior unique to the finite-thickness interfacial layer. Based on the differences in the physical origins of interfacial irreversible processes, the interfacial excess entropy production rate can be decoupled into two mutually independent contributory components, satisfying $\sigma_s=\sigma_s^{intra}+\sigma_s^{trans}$, thus enabling the quantitative differentiation between the two dissipative mechanisms, namely, internal interfacial evolution and cross-interface transport.

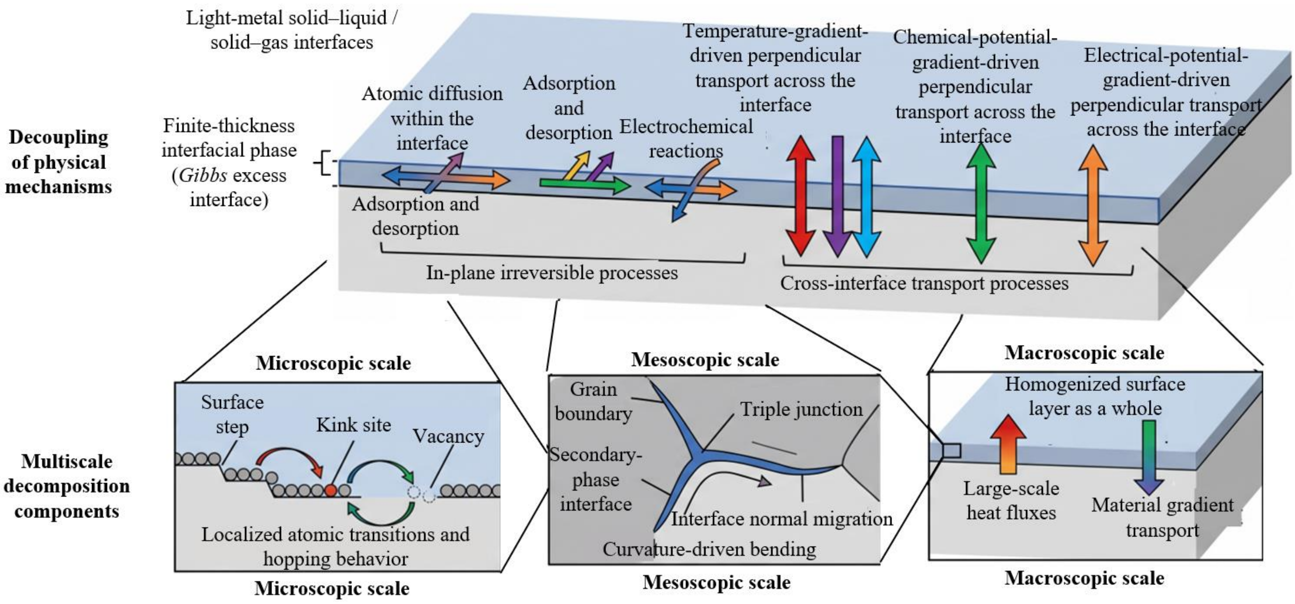

Figure 1. Schematic illustration of the decoupling of multiple physical mechanisms and multiscale decomposition of the interfacial excess entropy production rate for light-metal interfaces

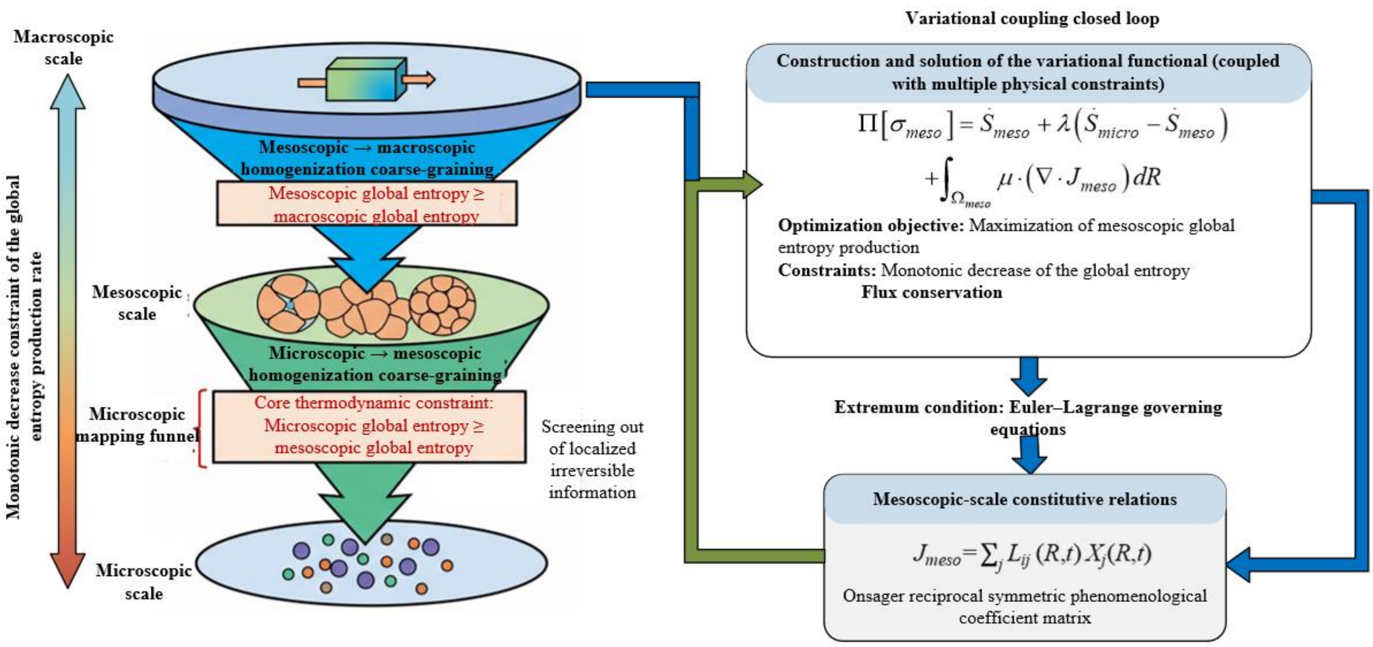

Figure 2. Cross-scale variational coarse-graining information transfer framework based on the constraint of monotonic entropy production decrease

The in-plane irreversible entropy production within the interface is governed by the microscopic dynamic behaviors occurring inside the interfacial layer, encompassing local processes such as surface atomic diffusion, interfacial adsorption and desorption, and in-situ electrochemical reactions, which constitute the primary source of energy dissipation arising from the spontaneous evolution of interfacial structures. The quantitative formulation for the in-plane entropy production constructed herein is given by:

$$\sigma_s^{intra}=J_s\cdot\nabla_s\mu_s+\sum_r\frac{A_r^s}{T}\xi_r^s \tag{2}$$

where, J_s and $\nabla_s\mu_s$ denote the surface diffusion flux and the surface gradient of chemical potential, respectively, and their vectorial coupling relationship precisely describes the irreversible dissipation associated with interfacial mass transport; A_r^s and ξ_r^s denote the interfacial reaction affinity and the reaction progress, respectively, which are employed to quantify the entropic contribution of multi-component interfacial chemical reactions, while the thermodynamic temperature T enables the normalized regulation of the reaction dissipation intensity by the temperature field. Cross-interface entropy production originates from the spatial discontinuity of the thermodynamic fields in the bulk phases; the abrupt variations of key physical parameters—including temperature, chemical potential, and electrical potential—across the two sides of the interface continuously drive heat transfer, mass transport, and charge transfer behaviors, with the corresponding entropy production characterization given by:

$$\sigma_s^{trans}=\sum_i J_i^{int}\cdot\Delta X_i \tag{3}$$

where, J_i^{int} denotes the cross-interface transport flux for each physical process, and ΔX_i denotes the difference across the interface of the corresponding generalized thermodynamic force; this formulation comprehensively covers all irreversible dissipation mechanisms associated with the cross-interface coupled transport of multiple physical fields in light-metal surface treatment.

The in-plane irreversible evolution of the interface simultaneously spans multiple spatial scales, namely, the microscopic, mesoscopic, and macroscopic scales, and characterization at a single scale is insufficient to fully reveal the global evolutionary patterns of interfacial entropy production. Based on the characteristic spatial scales of the physical processes, the in-plane entropy production rate is decomposed into three hierarchical levels, thereby establishing a multiscale synergistic characterization system, with the core decomposition relation given by:

$$\sigma_s^{intra}=\sigma_s^{atom}+\sigma_s^{meso}+\sigma_s^{macro} \tag{4}$$

Atomic-scale entropy production focuses on the dynamic evolution of microstructural features such as surface steps, kinks, and defect sites, with local atomic hopping behavior and chemical potential deviations employed as the core physical quantities, yielding a refined characterization model $\sigma_s^{atom}=\sum_\alpha \nu_\alpha\cdot\Delta\mu_\alpha/T$, through which the intrinsic energy dissipation at the microscopic scale is precisely quantified by the atomic jump frequency ν_α at distinct defect sites and the corresponding local chemical potential deviation $\Delta\mu_\alpha$. Mesoscopic entropy production addresses the migratory evolution of mesoscopic structures including grain boundaries, triple junctions, and secondary-phase interfaces; a computational model $\sigma_s^{meso}=\gamma\kappa\cdot v_n+J_{gb}\cdot\nabla_s\mu_{gb}$ is formulated by incorporating the coupled mechanisms of interface curvature-driven migration and grain-boundary diffusion, through which the irreversible dissipation associated with the deformation and migration of mesoscopic interfacial structures is characterized by means of the specific surface Gibbs free energy γ, the interface curvature vector κ, and the interface normal migration velocity v_n. Macroscopic entropy production corresponds to the overall field-evolution behavior of the homogenized surface layer, and its entropic characteristics for the global steady-state transport processes are represented through the coupled relationships among surface heat flux, material flux, and macroscopic field gradients.

Through this dual-level decomposition system, encompassing both physical mechanisms and spatial scales, a refined and full-dimensional analysis of the irreversible thermodynamic behavior at light-metal interfaces has been accomplished, thereby circumventing the inherent deficiencies of conventional models, including the lumped characterization of interfacial dissipation mechanisms and the confusion of scale coupling. By distinguishing the entropy production contributions of in-plane local evolution from those of cross-interface field transport, the respective proportions and evolutionary characteristics of the intrinsic and extrinsic irreversible dissipation at the interface can be precisely delineated, and the dominant roles of distinct physical processes in interfacial energy dissipation can be clearly elucidated. The three-tier scale decomposition model further enables the independent quantification of three distinct categories of physical processes—microscopic defect evolution, mesoscopic structural migration, and macroscopic field transport—thereby establishing an interfacial entropy production characterization system with matched scales and clearly defined mechanisms. The entire decomposition framework strictly adheres to the fundamental laws of nonequilibrium thermodynamics, and the conjugate relationships between generalized forces and generalized fluxes at each scale possess rigorous mathematical self-consistency, thereby providing a solid theoretical foundation for subsequent investigations, including thermodynamically constrained cross-scale modeling, analysis of entropy-variation laws at anisotropic interfaces, and thermodynamic optimization of process parameters.

3. CROSS-SCALE VARIATIONAL INFORMATION TRANSFER FRAMEWORK BASED ON THE GLOBAL POSITIVE DEFINITENESS OF THE ENTROPY PRODUCTION RATE

Through the multiscale decomposition method described above, the entropy production characteristics at different spatial scales can be independently quantified. However, the physical rationality of a multiscale modeling system is highly dependent on the self-consistency of information transfer between scales. Existing multiscale simulation frameworks for light-metal surface treatment have focused solely on the scale-matching fitting of mechanical parameters and transport properties, without incorporating the fundamental laws of nonequilibrium thermodynamics into the scale-coupling criteria, with the result that the coarse-graining procedures at each level fail to strictly comply with the second law of thermodynamics. Negative entropy production rates and physical-mechanism distortions are commonly encountered during scale ascent, severely compromising the predictive reliability of multiscale models. To address this issue, the global positive definiteness of the entropy production rate is imposed as the core physical constraint for cross-scale information transfer, and a multiscale coupling system with rigorous thermodynamic self-consistency is constructed. Figure 2 illustrates the cross-scale variational coarse-graining information transfer framework based on the constraint of monotonic entropy production decrease. The total entropy production at the microscopic scale can be expressed through spatial integration as:

$$\dot{S}_{micro}=\int_{\Omega}\sigma_{micro}(r,t)\,dr\geq 0 \tag{5}$$

where, $\sigma_{micro}(r,t)$ denotes the local microscopic entropy production rate density, r denotes the microscopic spatial coordinate, and Ω denotes the global computational domain of the system. This expression establishes, at the integral level, the fundamental physical criterion that must be satisfied throughout the multiscale evolutionary process.

The parameter mapping from the microscopic scale to the mesoscopic scale is essentially a homogenization coarse-graining process of microscopic degrees of freedom, during which the vast amount of refined physical information at the microscopic scale undergoes homogenized merging and dimensional reduction upon scale ascent. A standardized coarse-graining operator is introduced to achieve the regularized mapping of microscopic entropy production characteristics to the mesoscopic scale, with the scale transformation relation expressed as:

$$\sigma_{meso}(R,t)=C[\sigma_{micro}](R,t) \tag{6}$$

where, C denotes the coarse-graining operator from the microscopic to the mesoscopic scale, and R denotes the coarse-grained spatial coordinate at the mesoscopic scale. Scale coarse-graining inevitably filters out certain localized irreversible evolution information from the microscopic level, and the dissipative characteristics represented at the mesoscopic scale are merely the macroscopic statistical outcomes of the microscopic system; consequently, the global entropy production at the mesoscopic scale must always be less than or equal to that at the microscopic scale, with the corresponding constraint given by:

$$\dot{S}_{meso}=\int_{\Omega_{meso}}\sigma_{meso}(R,t)\,dR\leq\dot{S}_{micro} \tag{7}$$

This constraint fundamentally specifies the dissipative evolutionary behavior during scale ascent, thereby completely circumventing the deficiency inherent in conventional coarse-graining algorithms, namely, their violation of the fundamental laws of thermodynamics.

To select the optimal scale transformation model among all feasible coarse-graining mapping schemes, a variational functional coupled with multiple physical constraints is constructed by incorporating the monotonic decrease constraint of entropy production and the fundamental conservation laws of the medium:

$$\Pi[\sigma_{meso}]=\dot{S}_{meso}+\lambda\left(\dot{S}_{micro}-\dot{S}_{meso}\right)+\int_{\Omega_{meso}}\mu\cdot(\nabla\cdot J_{meso})\,dR \tag{8}$$

The functional takes the mesoscopic global entropy production as the optimization objective, with the Lagrange multiplier λ introduced to impose the scale-wise entropy constraint precisely, and the chemical potential vector μ introduced to enforce the flux conservation constraint, rigorously matching the local conservation rules for mass, energy, and charge, where J_{meso} denotes the generalized flux tensor at the mesoscopic scale. By applying the extremum condition $\delta\Pi=0$ to the functional, the Euler–Lagrange governing equations adapted to the multiscale coupling system can be derived. Through the solution of these equations, the constitutive relation between generalized forces and generalized fluxes at the mesoscopic scale is naturally obtained:

$$J_{meso}=\sum_{j}L_{ij}(R,t)\,X_j(R,t) \tag{9}$$

where, $L_{ij}(R,t)$ denotes the mesoscopic phenomenological coefficient matrix, which strictly satisfies the Onsager reciprocal symmetry. This constitutive relation is generated naturally through the variational principle without recourse to empirical parameter fitting, thereby ensuring the physical fidelity of the scale-wise constitutive relations.

Based on the variational theoretical framework for single-stage scale transformation, the thermodynamically self-consistent coarse-graining from the mesoscopic scale to the macroscopic scale can be implemented recursively, forming a complete multilevel information transfer chain. Through the sequential coarse-graining operators, the entropy production characteristics at the microscopic, mesoscopic, and macroscopic scales are regularly transformed and the corresponding parameters transferred, thereby establishing a closed-loop recursive coarse-graining chain. The entire scale-transformation process strictly adheres to the physical law of progressive entropy production decrease, satisfying the hierarchical constraint relation $\dot{S}_{macro}\leq\dot{S}_{meso}\leq\dot{S}_{micro}$. This framework embeds the second law of thermodynamics throughout all stages of multiscale modeling, enabling the unified and standardized derivation of constitutive relations between generalized forces and generalized fluxes across different scales, and resolving the core issues inherent in conventional multiscale simulations, namely, scale-coupling inconsistency and dissipative-mechanism distortion. Consequently, rigorous theoretical support is provided for the accurate quantification and mechanistic elucidation of multiscale irreversible thermodynamic behavior in light-metal surface treatment.

4. MESOSCOPIC-SCALE ENTROPY PRODUCTION MODEL CONSIDERING ANISOTROPIC INTERFACIAL THERMODYNAMIC PROPERTIES

The differences in crystal lattice symmetry of light metals induce a pronounced orientation dependence of interfacial thermodynamic parameters; the surface free energy and interfacial diffusion behavior of hexagonal close-packed magnesium alloys and preferentially oriented aluminum alloys exhibit significant anisotropic characteristics, which are fundamentally distinct from those of homogeneous isotropic material systems. Conventional mesoscopic entropy production models generally adopt a homogenized interface assumption, neglecting the regulatory effect of crystallographic orientation on the nonequilibrium evolution of the interface, and thus fail to accurately resolve the differentiated energy dissipation behaviors encountered during light-metal surface treatment processes. The rotational degrees of freedom of interfacial infinitesimal elements are incorporated into the nonequilibrium thermodynamic analysis framework, with the interface normal unit vector employed to characterize the crystallographic orientation state. An anisotropic specific surface Gibbs free energy quantification model adapted to the hexagonal close-packed lattice structure is established, and the orientation-dependent response of surface energy is precisely described through high-order polynomial fitting, with the specific expression given by:

$$\gamma(n)=\gamma_0\left[1+\epsilon_1\left(n_x^4+n_y^4+n_z^4-\frac{3}{5}\right)+\epsilon_2\, n_x^2 n_y^2 n_z^2\right] \tag{10}$$

where, γ_0 denotes the reference surface free energy corresponding to the basal-plane orientation, serving as the isotropic thermodynamic reference baseline; n_x, n_y, and n_z denote the components of the interface normal vector in the three-dimensional crystallographic coordinate system; and ϵ_1 and ϵ_2 denote the lattice anisotropy intensity coefficients, which can be determined through first-principles calculations or experimental calibration of material properties, and which quantitatively characterize the thermodynamic performance differences among distinct crystallographic planes. Figure 3 illustrates the mesoscopic thermodynamic evolution mechanisms at anisotropic interfaces of hexagonal close-packed light metals.

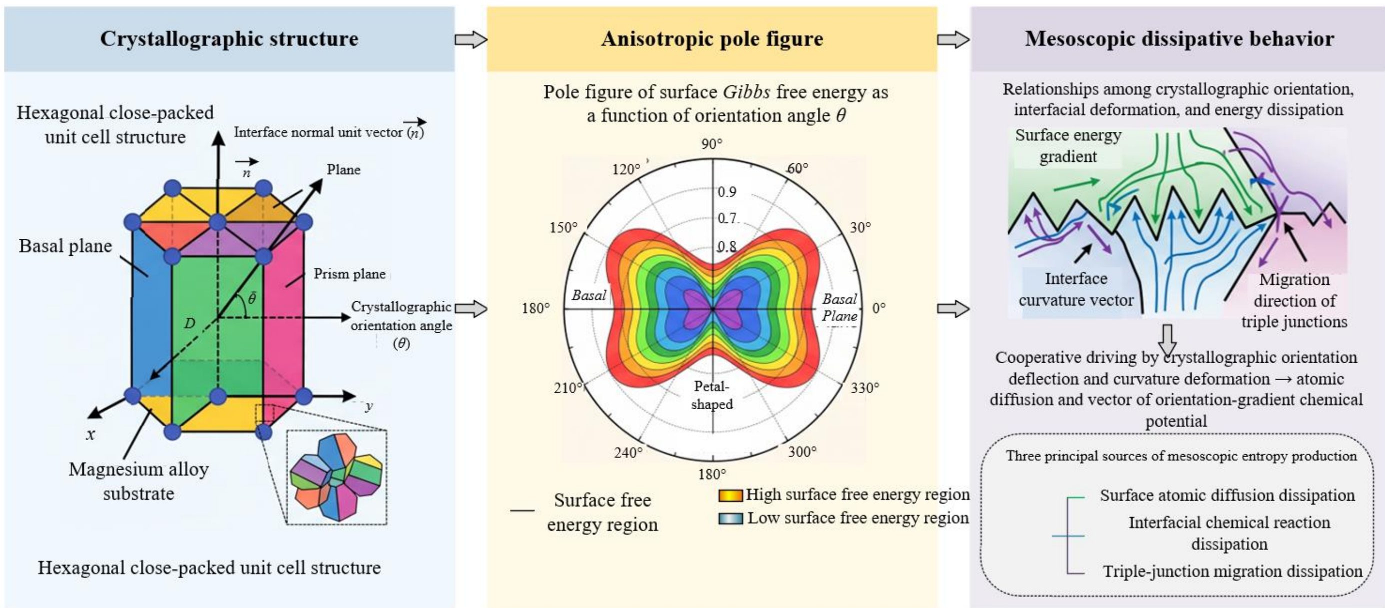

Figure 3. Mesoscopic thermodynamic evolution mechanisms at anisotropic interfaces of hexagonal close-packed light metals

During the dynamic evolution of the interface, crystallographic orientation deflection and interfacial curvature deformation cooperatively induce additional energy dissipation, which constitutes one of the core causes of irreversible entropy increase in anisotropic interface systems. Conventional interfacial chemical potential, which is formulated solely in terms of temperature and compositional concentration, fails to capture the thermodynamic driving-force variations arising from the coupling between crystallographic orientation and interfacial morphology. Through the coupling of the anisotropic surface energy gradient with the interfacial curvature effect, a refined expression for the mesoscopic interfacial chemical potential is reconstructed, and a direct correlation between crystallographic orientation evolution and thermodynamic driving behavior is established, with the expression given by:

$$\mu_s=\gamma(n)+\frac{\partial\gamma(n)}{\partial n}\cdot\kappa \tag{11}$$

where, κ denotes the interfacial mean curvature vector, which characterizes the bending deformation features of the interfacial microstructure. Based on the classical surface free energy, this formulation introduces a coupling term involving the partial derivative of surface energy with respect to the orientation vector, thereby incorporating both curvature-driven morphological migration and orientation-reconstruction-induced energy variations into a unified chemical-potential regulation framework, thus faithfully reproducing the physical essence of nonequilibrium evolution at anisotropic interfaces and providing accurate thermodynamic driving parameters for the quantitative computation of entropy production.

Based on the orientation-dependent interfacial chemical potential, a mesoscopic entropy production model that fully characterizes the dissipative features of anisotropic interfaces is constructed, comprehensively covering the three core irreversible processes in light-metal surface modification, namely, surface diffusion, interfacial chemical reactions, and triple-junction migration. The overall expression of the model is given by:

$$\sigma_s^{meso}(n)=J_{diff}\cdot\nabla_s\mu_s+J_{reac}\cdot A+J_{triple}\cdot F_{triple} \tag{12}$$

The first term in the formulation describes the entropic contribution of surface atomic diffusion, which is governed by the vectorial coupling between the surface diffusion flux and the orientation-gradient chemical potential, and directly reflects the regulatory effect of crystallographic orientation on the irreversible dissipation associated with interfacial mass transport. The second term characterizes the energy dissipation arising from interfacial electrochemical reactions; through the conjugate matching of reaction fluxes with chemical reaction affinities, the entropic characteristics induced by differences in interfacial reaction kinetics under distinct crystallographic orientations are quantified. The third term addresses the polycrystalline light-metal interfacial structure by describing the irreversible dissipation generated by the dynamic motion of triple junctions, which are the intersections of grain boundaries with the free surface; through the coupling between the junction migration flux and the corresponding thermodynamic force, the full-domain characterization capability for mesoscopic entropy production in polycrystalline systems is thereby enhanced.

To elucidate the quantitative correlation mechanism between crystallographic orientation angle and interfacial entropy production, a two-dimensional cross-sectional simplification of the three-dimensional anisotropic thermodynamic model is performed, with the interface normal vector expressed as a function of the orientation angle. Substitution into the general chemical-potential expression yields the orientation-angle-dependent simplified model:

$$\mu_s(\theta) = \gamma(\theta) - \gamma''(\theta)\cdot\kappa \tag{13}$$

where, $\gamma''(\theta)$ denotes the second-order derivative of the orientation-dependent surface energy with respect to the orientation angle, the magnitude of which directly defines the degree of interfacial crystallographic anisotropy. The stronger the interfacial anisotropy, the more significant the lattice-structure reconstruction induced by crystallographic orientation deflection, and the greater the corresponding entropy production increment during interfacial evolution. This modeling framework overcomes the representational limitations of conventional mesoscopic thermodynamic models, which assume homogenization and absence of orientation dependence, by fully incorporating crystallographic anisotropy into the nonequilibrium entropy-variation analysis system, and establishes a precise quantitative relationship among crystallographic orientation, interfacial deformation, and energy dissipation, thereby providing rigorous thermodynamic theoretical support for mechanism analysis and process optimization of anisotropic light-metal surface treatment.

5. ENTROPY PRODUCTION MAPS AND EXPERIMENTAL VALIDATION FOR TYPICAL LIGHT-METAL SURFACE TREATMENT PROCESSES

5.1 Multiscale entropy production rate model

The multiscale decomposition rules, cross-scale thermodynamic constraint framework, and anisotropic interfacial entropy-variation theory established above provide comprehensive theoretical support for quantifying the energy dissipation mechanisms in light-metal surface treatment. To adapt and implement the purely theoretical model within engineering process systems, anodizing of aluminum alloys and micro-arc oxidation of magnesium alloys were selected as representative case studies. All irreversible evolutionary behaviors arising from the coupling of multiple physical fields within the two process systems—including Joule-heat-induced thermal conduction dissipation, ion migration dissipation at the oxide-film/electrolyte interface, interfacial electrochemical reaction dissipation, and localized strong transient dissipation induced by micro-arc discharge—were systematically incorporated, and a globally coupled multiscale total entropy production rate model was constructed:

$$\begin{aligned}\dot{S}_{total}= & \int_V \frac{J_q\cdot\nabla T}{T^2}\,dV+\int_V\sum_k J_k\cdot\left(-\nabla\frac{\mu_k}{T}\right)dV \\ & +\int_{A_s}\sum_r\frac{A_r}{T}\xi_r\,dA+\dot{S}_{plasma}\end{aligned} \tag{14}$$

where, the first term denotes the entropic contribution of thermal conduction in the bulk phase, with the irreversible dissipation of heat transport characterized through the coupling between heat flux and temperature gradient; the second term denotes the entropic contribution of multicomponent mass diffusion, with the energy dissipation during ion migration quantified via chemical potential gradients; the third term denotes the entropic contribution of interfacial chemical reactions, with the entropy-variation characteristics of interfacial electrochemical reactions described through the dynamic correlation between reaction affinity and reaction progress; and the fourth term denotes the transient entropic contribution of plasma spark discharge, for which the mesoscopic information extraction and quantification are accomplished through the variational coarse-graining framework established previously. This formulation overcomes the limitation of conventional models, which are restricted to describing steady-state weakly nonequilibrium processes, and achieves an integrated thermodynamic characterization encompassing both steady-state transport processes and transient strongly nonequilibrium discharge events.

5.2 Numerical solution methodology for entropy production maps

The multiscale entropy production model encompasses physical information across atomic, mesoscopic, and macroscopic levels, and a single numerical algorithm is incapable of accommodating both the scale disparities and the thermodynamic self-consistency requirements. To address this challenge, a hierarchically coupled multiscale collaborative solution strategy was established. Through density functional theory calculations, the atomic-scale material property parameters were calibrated, enabling the accurate acquisition of orientation-dependent surface free energies, atomic diffusion energy barriers, and intrinsic reaction pathways for distinct crystallographic planes, which serve as the fundamental material-property inputs for mesoscopic evolution computations. Based on the parameters calibrated at the atomic scale, the phase-field method was employed to solve the governing equations for mesoscopic interface evolution, reproducing the spatiotemporal evolutionary characteristics of interfacial morphology, concentration fields, and temperature fields, and accomplishing the refined computation of mesoscopic entropy production distributions at anisotropic interfaces. Through the thermodynamically self-consistent constitutive relations obtained from mesoscopic coarse-graining, the macroscopic governing equations for coupled multiple physical fields were solved via the finite-element method, thereby achieving the full-domain computation of bulk-phase entropy production. The information transfer across multiple scales strictly adhered to the constraint criterion of monotonic entropy production decrease, thereby completely circumventing the thermodynamic incompatibility issues inherent in conventional multiscale simulations. Ultimately, spatiotemporally resolved entropy production distribution maps were obtained through the solution procedure, enabling the precise revelation of spatial hot-spot distributions and dynamic evolutionary patterns of irreversible dissipation during light-metal surface treatment processes. Figure 4 presents the coupled solution architecture for the multiscale entropy production contour maps of anodizing and micro-arc oxidation.

5.3 Experimental design and validation protocol

To hierarchically validate the predictive accuracy and applicability range of the multiscale entropy production theoretical framework, five groups of controlled experiments were designed from four dimensions: steady-state anodizing, pulsed micro-arc oxidation, crystallographic orientation effects, and process parameter optimization. Quantitative validation was conducted respectively for thermal transport dissipation, dynamic interfacial reactions, plasma-driven strongly nonequilibrium processes, interfacial anisotropy, and thermodynamic process criteria. In each experimental group, process control parameters, in-situ multifield signals, and coating microstructural characterization results were simultaneously acquired, and the entropy production values for each component under the corresponding operating conditions were computed using the multiscale model established above. The complete test datasets are compiled in Tables 1 through 5.

Table 1 records the complete quantitative data for the steady-state stage of constant-current anodizing, which were used to validate the thermal conduction entropy production sub-model. Under fixed electrolyte composition and temperature conditions, the increase in current density simultaneously enhanced the Joule heating power of the system, and the thermal conduction entropy production rate output by the model exhibited a linearly positive correlation with the measured thermal power, with the relative prediction errors of the model maintained within 4% across all operating conditions. The observed data trends confirm that thermal irreversible dissipation constitutes the core component of entropy production in constant-current anodizing systems, while also demonstrating that the integral-form thermal entropy production model established herein accurately captures the energy dissipation characteristics of steady-state heat transport processes.

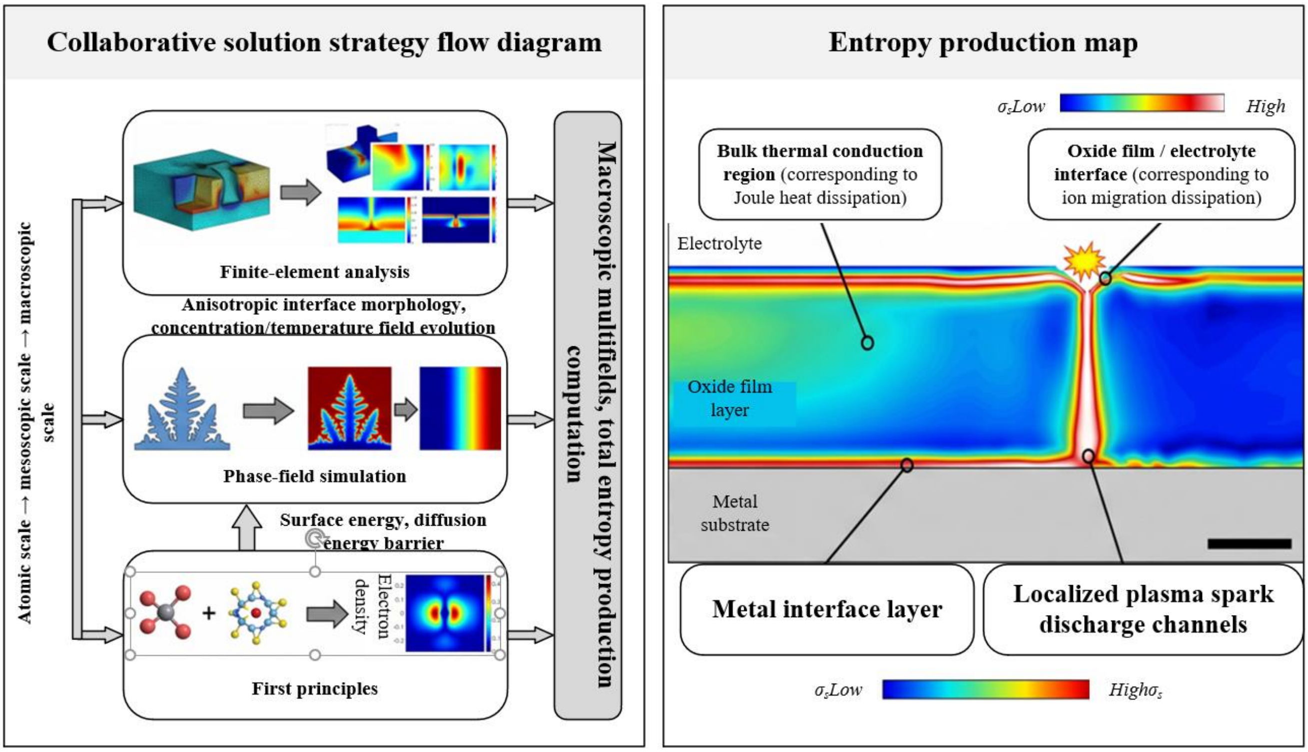

Figure 4. Coupled solution architecture for multiscale entropy production contour maps of anodizing and micro-arc oxidation

Table 1. Operating conditions and quantitative test results for constant-current anodizing of AA6061 in a sulfuric acid system

Experimental Group	Current Density ($mA\cdot cm^{-2}$)	Electrolyte Temperature (°C)	Sulfuric Acid Mass Fraction (%)	Steady-State Cell Voltage (V)	Average Coating Thickness (μm)	Measured Joule Heating Power ($W\cdot m^{-2}$)
S1	10	20	10	11.2	6.1	186.4
S2	20	20	15	13.5	8.7	362.1
S3	30	30	15	16.8	11.3	547.6
S4	40	30	20	19.4	13.6	731.2
S5	50	40	20	22.7	15.8	924.8

Table 2. Experimental data for dynamic evolution of constant-voltage anodizing of AA2024 in oxalic acid system

Experimental Group	Applied Voltage (V)	Electrolyte Temperature (℃)	Oxalic Acid Mass Fraction (%)	Steady-State Terminal Current ($A\cdot m^{-2}$)	Coating Growth Rate ($\mu m\cdot min^{-1}$)	Interfacial Reaction Entropy Production in Later Oxidation Stage ($J\cdot K^{-1}\cdot m^{-2}\cdot s^{-1}$)	Coating Surface Roughness (nm)
P1	15	15	3	12.4	0.142	0.021	76.3
P2	20	20	4	9.7	0.118	0.017	62.5
P3	20	30	4	7.2	0.094	0.013	51.8
P4	25	25	5	6.5	0.081	0.01	44.2
P5	30	35	5	4.1	0.056	0.006	32.7

Table 3. Multifield coupled test dataset for pulsed micro-arc oxidation of AZ91D magnesium alloy

Experimental Group	Pulse Voltage (V)	Pulse Frequency (Hz)	Duty Cycle (%)	Average Surface Peak Temperature (℃)	Plasma Entropy Production Fraction in Total Entropy (%)	Total Entropy Production Rate ($J\cdot K^{-1}\cdot m^{-2}\cdot s^{-1}$)	Average Energy per Single Discharge (mJ)
M1	300	100	10	426	18.3	0.316	12.4
M2	380	300	20	472	27.5	0.428	18.6
M3	420	500	30	518	36.2	0.547	24.3
M4	460	800	40	564	45.7	0.662	29.8
M5	500	1000	50	613	54.1	0.785	36.2

Table 4. Mesoscopic entropy production and coating characterization results for pure magnesium samples with different crystallographic orientations

Crystallographic Orientation	Interface Normal Vector	Average Coating Thickness (μm)	Coating Thickness Standard Deviation (μm)	Surface Diffusion Entropy Production ($J\cdot K^{-1}\cdot m^{-2}\cdot s^{-1}$)	Total Mesoscopic Entropy Production $\sigma_s^{meso}(n)$	Surface Energy Parameter $\gamma(n)$ ($J\cdot m^{-2}$)
Basal (0001)	(0,0,1)	9.2	0.41	0.046	0.083	0.426
Prism (101¯0)	(1,0,0)	6.7	1.15	0.078	0.137	0.489
Prism (112¯0)	(1,1,0)	5.9	1.43	0.091	0.152	0.514

Table 5. Response surface orthogonal experimental parameters, total entropy production, and comprehensive coating performance for AA7075

Experimental Group	Current Density ($mA\cdot cm^{-2}$)	Electrolyte Temperature (℃)	Treatment Duration (min)	Global Total Entropy Production $\dot{S}_{total}$	Coating Microhardness (HV)	Corrosion Current Density ($\mu A\cdot cm^{-2}$)	Coating Thickness Uniformity Coefficient
O1	15	20	30	0.274	362	1.86	0.91
O2	25	25	40	0.218	427	1.13	0.95
O3	35	30	50	0.342	384	2.41	0.87
O4	25	30	30	0.186	456	0.72	0.97
O5	25	20	50	0.249	403	1.47	0.93
O6	35	25	30	0.305	371	2.09	0.89

Table 2 focuses on the dynamic entropic characteristics throughout the entire coating growth process under constant-voltage conditions. With increasing applied voltage, the impedance of the oxide film continuously increased, the steady-state current of the system gradually decayed, and the entropy production corresponding to the interfacial electrochemical reactions decreased concomitantly, while both the coating growth rate and surface roughness declined synchronously. The variation amplitude of the interfacial reaction entropy production computed by the model exhibited a high degree of consistency with the evolutionary patterns of the coating microstructure, indicating that the model is capable of fully capturing the irreversible dissipation variations resulting from the attenuation of reaction kinetics during the middle and late stages of anodizing.

To investigate the anisotropic distribution of mesoscopic interfacial entropy production during light-metal surface modification and its regulatory effect on local coating morphology, the following experimental analysis was conducted. The composite image of electron backscatter diffraction mapping and phase-field simulation contour maps, as shown in Figure 5, clearly reveals the strong dependence of the initial crystallographic orientation of the magnesium alloy on the interfacial dissipation hotspots. In contrast to the interior of low-dissipation basal-oriented grains characterized by lower surface free energy, the interior of high-dissipation prismatic grains, as well as grain boundaries and triple-junction regions, all exhibited extremely high local interfacial entropy production rates. In-situ scanning electron microscopy morphological micrographs directly verified the decisive influence of this thermodynamic dissipation mechanism on morphological evolution, in that the high-dissipation red hotspot regions in the simulation contour maps corresponded precisely to the regions where coating surface roughness, defects, and preferential pore nucleation occurred. Quantitative curves extracted across grain boundaries further solidified this inverse correlation, in that the peaks of local entropy production rates were accompanied by anomalous fluctuations in measured local coating thickness and morphological nonuniformity, thereby strongly confirming that non-equilibrium mesoscopic dissipation, driven by crystallographic anisotropy and structural defects, constitutes the underlying irreversible thermodynamic root cause of quality deterioration in the local evolution of oxide films on light metals.

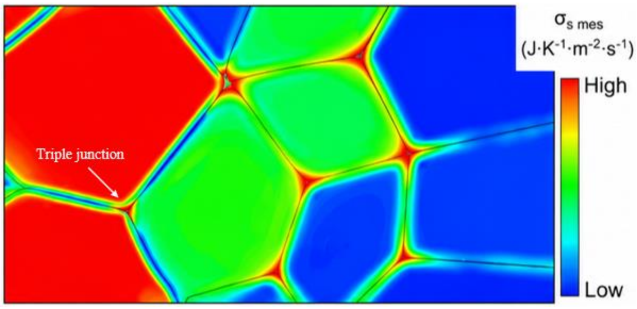

(a) Phase-field simulation contour map of mesoscopic interfacial entropy production rate

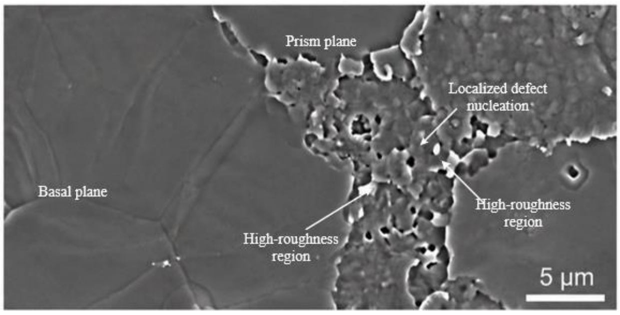

(b) In-situ morphological evolution micrograph of the corresponding region

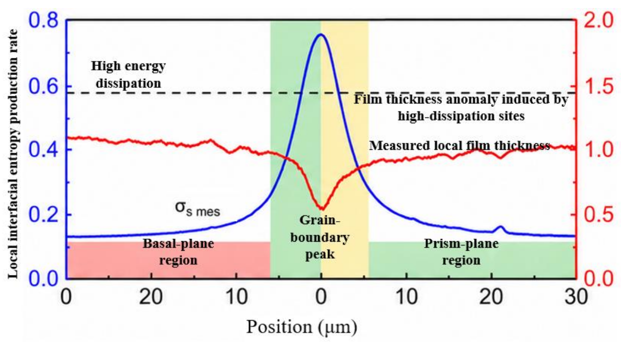

(c) Entropy production versus film thickness correlation curves extracted across grain boundaries

Figure 5. Spatial distribution of mesoscopic entropy production driven by crystallographic orientation and interfacial defects and its morphological correlation map

Table 3 quantitatively characterizes the transient strongly nonequilibrium entropy production arising from plasma discharge during micro-arc oxidation. With the simultaneous increase of pulse voltage, frequency, and duty cycle, the spark discharge frequency and the energy released per pulse increased significantly, and the plasma entropy production fraction in the total entropy rose from 18.3% to 54.1%, becoming the dominant source of irreversible dissipation under high-voltage operating conditions. The $\dot{S}_{plasma}$ component, obtained through the solution of the variational coarse-graining framework established in Section 4, was capable of quantitatively reproducing the coupling relationship between discharge parameters and transient dissipation, thereby filling the deficiency of conventional steady-state thermodynamic models, which are incapable of describing plasma-driven strongly nonequilibrium processes.

Table 4 is employed to validate the anisotropic mesoscopic entropy production model established in Section 4. Under identical process conditions, the basal-oriented samples exhibited lower surface free energy, and the irreversible entropy production corresponding to interfacial diffusion was significantly lower than that of the two prismatic orientations, with the total mesoscopic entropy production demonstrating a pronounced gradient variation as a function of crystallographic orientation. The prismatic crystal planes possessed higher atomic migration energy barriers, resulting in stronger energy dissipation during interfacial evolution and a concomitant deterioration in coating thickness uniformity. The experimental data were in complete agreement with the entropy-variation laws derived from the orientation-dependent chemical potential, thereby verifying the rationality of incorporating interfacial rotational degrees of freedom into the thermodynamic framework.

Table 5 presents the response surface orthogonal optimization experimental dataset, establishing the quantitative correlations among process parameters, global total entropy production, and coating service performance. The target oxide coating thickness was maintained consistently across all experimental groups, with only the three core variables—current density, temperature, and treatment duration—being varied. Comparison of the data across all operating conditions reveals that Group O4 exhibited the lowest global total entropy production value, while simultaneously yielding the highest microhardness, the lowest corrosion current density, and the optimal coating thickness uniformity. A clear negative correlation was observed between the level of irreversible energy dissipation and the comprehensive coating performance, thereby providing direct experimental support for the thermodynamic process optimization criteria.

To further validate the physical self-consistency and technical accuracy of the proposed multiscale irreversible thermodynamic analysis framework for light-metal surface treatment, particularly in terms of scale coarse-graining and transient multifield coupled descriptions, the following experimental analysis was conducted. The cross-scale monotonic entropy production decrease step chart, as shown in Figure 6, clearly presents the progressive decreasing trend of the global entropy production rate from the microscopic scale to the mesoscopic scale and then to the macroscopic scale under specific steady-state anodizing conditions. The dissipation loss between each pair of adjacent scales precisely quantifies the dissipation resulting from the filtering out of high-frequency fluctuation information during the corresponding scale-ascent coarse-graining procedure, thereby strictly verifying, at the overall system level, that the multilevel coarse-graining process adheres to the fundamental thermodynamic law of monotonic entropy production decrease. The real-time evolutionary curves of multiscale energy dissipation over a transient micro-arc discharge cycle further extended this multiscale description to strongly nonequilibrium processes. By demonstrating that the transient mesoscopic oscillation curves, computed from locally sampled high-frequency data, were perfectly enveloped by the macroscopic equivalent dissipation curves computed from smoothed macroscopic electrical signals, the smoothing mechanism of mesoscopic dissipative oscillations at the macroscopic scale was revealed, thereby confirming the technical accuracy of the cross-scale information transfer pathway established in the transient coupled model.

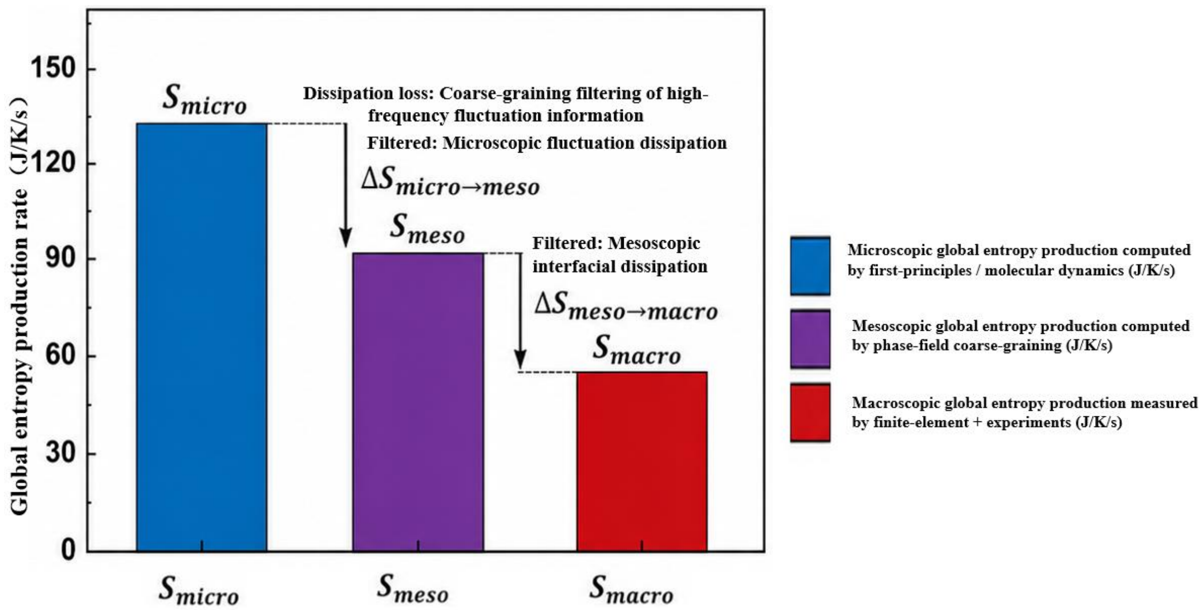

(a) Cross-scale monotonic entropy production decrease step chart

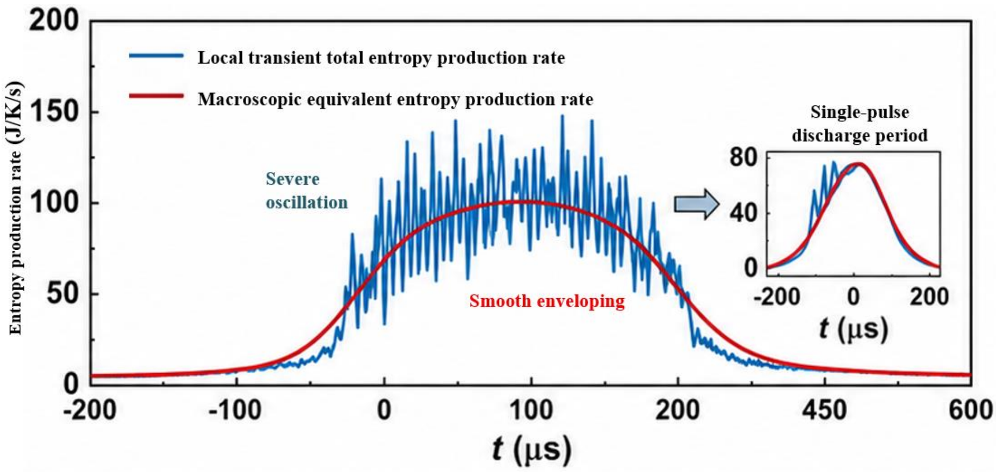

(b) Real-time evolutionary curves of multiscale energy dissipation over a transient micro-arc discharge cycle

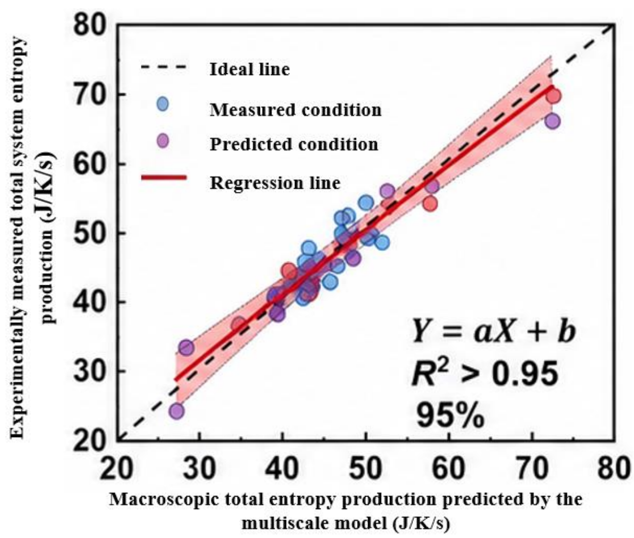

(c) Error scatter plot of macroscopic total entropy production between experiments and multiscale model predictions

Figure 6. Validation of thermodynamic self-consistency in multiscale information transfer and the law of monotonic entropy production decrease

5.4 Thermodynamic process optimization criteria

Based on the complete quantitative data from the five preceding experimental groups and the computed multiscale entropy production results, and grounded in the nonequilibrium thermodynamic principle of minimum entropy production, optimization criteria for light-metal surface treatment parameters were established. Under fixed engineering constraints—including coating thickness, treatment duration, and equipment energy consumption—the optimal process parameter combination corresponds to the global total entropy production of the system attaining its minimum value, with the mathematical formulation expressed as:

$$\min_{p \in P} \dot{S}_{total}(p; constraints) \tag{15}$$

where, p denotes the process parameter vector consisting of current density, applied voltage, electrolyte temperature, pulse frequency, and duty cycle, and P denotes the feasible parameter space satisfying engineering processing constraints.

A mechanistic analysis was conducted in conjunction with the orthogonal experimental data presented in Table 5. The global entropy production value quantitatively represents the total irreversible energy dissipation per unit coating growth. A lower entropy production value indicates that a smaller fraction of the input electrical energy is converted into useless heat, interfacial defects, and plasma dissipation, while the utilization efficiency of energy conversion toward the formation of a dense protective oxide film is correspondingly higher. High current density and elevated electrolyte temperature simultaneously exacerbate ion diffusion, Joule heat loss, and non-uniform interfacial reactions, thereby directly raising the total system entropy production and leading to increased internal coating defects and degraded corrosion resistance. Conversely, excessively low parameter values prolong the treatment duration and introduce additional time-dimensional energy dissipation, also causing an increase in total entropy production. Only when the three categories of process parameters reach a synergistic matching regime do the various irreversible entropy production components of the system simultaneously decrease to relatively low levels, thereby establishing the optimal process window.

Based on the fitting of all operating-condition data from Tables 1 through 5, the low-entropy parameter intervals for the two process categories—anodizing of aluminum alloys and micro-arc oxidation of magnesium alloys—can be delineated. For the anodizing system, the optimal parameter interval is identified as a current density of 20–30 $mA \cdot cm^{-2}$ and an electrolyte temperature of 25–30 °C; for the micro-arc oxidation system, the low-dissipation interval is defined by a pulse voltage of 380–440 V and a duty cycle of 20%–35%. This optimization criterion is constructed entirely on the basis of the underlying laws of irreversible thermodynamics, in contrast to conventional approaches that rely on trial-and-error optimization based on single performance indicators. It enables the quantitative and rapid screening of multi-objective process parameters, thereby providing a standardized thermodynamic analytical pathway for the development of low-energy, high-performance light-metal surface modification processes.

6. CONCLUSIONS

A multiscale irreversible thermodynamic analytical framework tailored to the interfacial characteristics of light-metal surface modification was systematically constructed, and the theoretical representations for entropy variation at anisotropic nonequilibrium interfaces and for cross-scale coupling mechanisms were advanced. Based on the Gibbs excess theory, the physical mechanisms of interfacial entropy production were decoupled and decomposed across spatial scales, enabling the precise decoupling and quantification of two categories of dissipative behaviors—in-plane interfacial evolution and cross-interface transport—as well as the irreversible characteristics across three scales, namely, atomic, mesoscopic, and macroscopic. By imposing the global positive-definiteness constraint on the entropy production rate, a thermodynamically self-consistent cross-scale variational information transfer framework was established, and the constitutive relations between generalized forces and generalized fluxes at each scale were rigorously derived through variational principles, thereby resolving, from a theoretical standpoint, the pervasive issues of missing thermodynamic constraints and scale-coupling inconsistency in conventional multiscale simulations. Through the incorporation of interfacial rotational degrees of freedom, an orientation-dependent mesoscopic entropy production model was developed, effectively revealing the quantitative regulatory effects of crystallographic anisotropy on the irreversible evolution and energy dissipation at light-metal interfaces, and remedying the theoretical deficiency that homogenized thermodynamic models are incapable of accommodating the crystallographic characteristics of light metals.

In conjunction with the typical engineering processes of anodizing of aluminum alloys and micro-arc oxidation of magnesium alloys, a comprehensive multiscale entropy production computational model was established, encompassing steady-state transport, interfacial chemical reactions, and transient plasma discharge, and an entropy production mapping methodology capable of characterizing the spatiotemporal evolutionary features of interfacial dissipation was developed. Based on the principle of minimum entropy production, a novel thermodynamic process optimization criterion was established, specifying the correspondence between the optimal process parameters under given constraints and the minimum entropy dissipation of the system. Through multiple groups of hierarchical controlled experiments, the accuracy of the theoretical models and the feasibility of the optimization methodology were fully validated. This investigation overcomes the limitations of idealized conventional interfacial thermodynamic analyses and the disconnection between theoretical mechanisms and engineering applications, enriches the nonequilibrium irreversible thermodynamic theory for light-metal interfaces, and provides solid theoretical support and scientific foundations for the improvement of energy efficiency and the precise regulation of coating performance in surface treatment of high-end light-metal components.

REFERENCES

[1] Tan, J., Ramakrishna, S. (2021). Applications of magnesium and its alloys: A review. Applied Sciences, 11(15): 6861. https://doi.org/10.3390/app11156861

[2] Bai, J., Yang, Y., Wen, C., et al. (2023). Applications of magnesium alloys for aerospace: A review. Journal of Magnesium and Alloys, 11(10): 3609-3619. https://doi.org/10.1016/j.jma.2023.09.015

[3] Ali, M., Elsherif, M., Salih, A.E., et al. (2020). Surface modification and cytotoxicity of Mg-based bio-alloys: An overview of recent advances. Journal of Alloys and Compounds, 825: 154140. https://doi.org/10.1016/j.jallcom.2020.154140

[4] Yao, W., Tan, Y., Lu, Q., et al. (2024). Recent advances in protective coatings and surface modifications for corrosion protection of Mg alloys. Journal of Materials Research and Technology, 31: 3238-3254. https://doi.org/10.1016/j.jmrt.2024.07.046

[5] Daroonparvar, M., Bakhsheshi-Rad, H.R., Saberi, A., et al. (2022). Surface modification of magnesium alloys using thermal and solid-state cold spray processes: Challenges and latest progresses. Journal of Magnesium and Alloys, 10(8): 2025-2061. https://doi.org/10.1016/j.jma.2022.07.012

[6] Chaharmahali, R., Fattah-alhosseini, A., Babaei, K. (2021). Surface characterization and corrosion behavior of calcium phosphate (Ca-P) base composite layer on Mg and its alloys using plasma electrolytic oxidation (PEO): A review. Journal of Magnesium and Alloys, 9(1): 21-40. https://doi.org/10.1016/j.jma.2020.07.004

[7] Fattah-alhosseini, A., Chaharmahali, R., Babaei, K. (2020). Effect of particles addition to solution of plasma electrolytic oxidation (PEO) on the properties of PEO coatings formed on magnesium and its alloys: A review. Journal of Magnesium and Alloys, 8(3): 799-818. https://doi.org/10.1016/j.jma.2020.05.001

[8] Di Giuseppe, A., Rossi, F. (2025). Thermophysical assessment of high-albedo surfaces for solar radiation management and equivalent energy impact evaluation. Power Engineering and Engineering Thermophysics, 4(4): 228-234. https://doi.org/10.56578/peet040402

[9] Maroto, J.C., Muñoz, S., Barragán, V.M. (2024). Entropy production in an electro-membrane process at underlimiting currents—Influence of temperature. Entropy, 27(1): 3. https://doi.org/10.3390/e27010003

[10] Hafskjold, B., Bedeaux, D., Kjelstrup, S., Wilhelmsen, Ø. (2021). Theory and simulation of shock waves: Entropy production and energy conversion. Physical Review E, 104(1): 014131. https://doi.org/10.1103/PhysRevE.104.014131

[11] Jing, X., Wang, Q. (2022). Thermodynamically consistent models for coupled bulk and surface dynamics. Entropy, 24(11): 1683. https://doi.org/10.3390/e24111683

[12] Prahs, A., Schneider, D., Nestler, B. (2025). A continuum thermodynamic approach to the phase-field method: The order parameter as internal state variable. Continuum Mechanics and Thermodynamics, 37(4): 55. https://doi.org/10.1007/s00161-025-01383-y

[13] Bothe, D. (2022). Sharp-interface continuum thermodynamics of multicomponent fluid systems with interfacial mass. International Journal of Engineering Science, 179: 103731. https://doi.org/10.1016/j.ijengsci.2022.103731

[14] Rauscher, P.M., Öttinger, H.C., de Pablo, J.J. (2022). Nonequilibrium statistical thermodynamics of multicomponent interfaces. Proceedings of the National Academy of Sciences, 119(24): e2121405119. https://doi.org/10.1073/pnas.2121405119

[15] Masi, F., Stefanou, I. (2022). Multiscale modeling of inelastic materials with Thermodynamics-based Artificial Neural Networks (TANN). Computer Methods in Applied Mechanics and Engineering, 398: 115190. https://doi.org/10.1016/j.cma.2022.115190

[16] Sekkal, S.E., Idrissi, M.E.F., Meraghni, F., Chatzigeorgiou, G., Chinesta, F. (2025). Multiscale Thermodynamics-Informed Neural Networks (MuTINN) for nonlinear structural computations of recycled thermoplastic composites. Composites Part B: Engineering, 300: 112455. https://doi.org/10.1016/j.compositesb.2025.112455

[17] Teza, G., Stella, A.L. (2020). Exact coarse graining preserves entropy production out of equilibrium. Physical Review Letters, 125(11): 110601. https://doi.org/10.1103/PhysRevLett.125.110601

[18] Cocconi, L., Salbreux, G., Pruessner, G. (2022). Scaling of entropy production under coarse graining in active disordered media. Physical Review E, 105(4): L042601. https://doi.org/10.1103/PhysRevE.105.L042601

[19] Bai, S., Jiang, B., He, W., et al. (2024). Orientation engineering of magnesium alloy: A review. Journal of Materials Research and Technology, 33: 4908-4937. https://doi.org/10.1016/j.jmrt.2024.10.121

[20] Yamasaki, M., Shi, Z., Atrens, A., Furukawa, A., Kawamura, Y. (2022). Influence of crystallographic orientation and Al alloying on the corrosion behaviour of extruded α-Mg/LPSO two-phase Mg-Zn-Y alloys with multimodal microstructure. Corrosion Science, 200: 110237. https://doi.org/10.1016/j.corsci.2022.110237

[21] Long, M., Charoen-amornkitt, P., Alizadeh, M., Suzuki, T., Tsushima, S. (2025). Design principle for topography-optimized porous reactors: Entropy generation minimization and equipartition of entropy production. International Journal of Heat and Mass Transfer, 245: 127000. https://doi.org/10.1016/j.ijheatmasstransfer.2025.127000